ACCSCIENCE PUBLISHING

International Journal of Bioprinting

RESEARCH ARTICLE

Melt electrospinning writing PCL scaffolds after alkaline modification with outstanding cytocompatibility and osteoinduction

Yubo Shi[1†], Lei Wang[1†], Liguo Sun[2†], Zhennan Qiu[3,4], Xiaoli Qu[3,4], Jingyi Dang[1], Zhao Zhang[1], Jiankang He[3,4*], and Hongbin Fan[1*]

[1]Department of Orthopedic Surgery, Xijing Hospital, The Fourth Military Medical University, Xi'an, China

[2]Department of Medical Management, Shaanxi Provincial Hospital of Chinese Medicine, Xi'an, China

[3]State Key Laboratory for Manufacturing Systems Engineering, Xi'an Jiaotong University, Xi'an, China

[4]Rapid Manufacturing Research Center of Shaanxi Province, Xi'an Jiaotong University, Xi'an, China

Abstract

Melt electrospinning writing (MEW) is a promising three-dimensional (3D) printing technology that enables the creation of scaffolds with highly ordered microfibers. Polycaprolactone (PCL) is an ideal material for MEW scaffold fabrication due to its exceptional printability. However, its low cellular affinity can hinder its performance in bone tissue engineering. This study aimed to explore the potential of NaOH treatment as a means of enhancing the cytocompatibility and osteoinductive properties of PCL scaffolds. After modification with a NaOH solution, the physiochemical properties of the MEW PCL scaffold were analyzed. The surface of the scaffold was found to have nanopits and nanogrooves, which differed from the smooth surface of the PCL scaffold. Atomic force microscopy and automatic water contact angle assays revealed an increase in surface roughness and wettability, both of which were found to be beneficial for cell proliferation and adhesion. *In vitro* experiments demonstrated that the NaOH-treated surface was able to induce osteogenic differentiation of rat bone marrow mesenchymal stem cells (BMSCs) via the integrinα2/β1-PI3K-Akt signaling pathway, which had not been previously observed. The study involved implanting PCL scaffold to repair a cranial defect. After 1 and 3 months of implantation, histological analysis and micro-computed tomography scans showed a higher amount of newly formed bone on the NaOH-treated PCL scaffolds compared to the PCL scaffold. The study concluded that NaOH treatment was a simple and effective way to enhance cellular affinity and osteoinductive property of MEW PCL scaffold. This strategy may provide a cost-efficient method for promoting bone regeneration.

Keywords: Melt electrospinning writing; Polycaprolactone; Bone regeneration; Tissue engineering

[†]These authors contributed equally to this work.

***Corresponding authors:**
Hongbin Fan (fanhb@fmmu.edu.cn)

Jiankang He (jiankanghe@mail.xjtu.edu.cn)

Citation: Shi Y, Wang L, Sun L, *et al*., 2023, Melt electrospinning writing PCL scaffolds after alkaline modification with outstanding cytocompatibility and osteoinduction. *Int J Bioprint*, 9(6): 1071. https://doi.org/10.36922/ijb.1071

Received: June 12, 2023
Accepted: July 13, 2023
Published Online: August 11, 2023

1. Introduction

Craniofacial bone defects not only have a serious impact on the patient's quality of life but also represent a challenge for surgeon[1]. The clinical treatments for craniofacial bone defects mainly include autogenous grafts, allogeneic grafts, and engineered bone[2]. Despite being the standard treatment for bone defects, autograft is limited by a lack of tissue source. Although allogeneic bone is widely used, it carries the risk of immune rejection and disease transmission[3,4]. In this context, engineered bone shows great potential for the treatment of bone defects[5-7].

Melt electrospinning writing (MEW) is an innovative three-dimensional (3D) printing technique that enables the creation of structures with precisely arranged microfibers, making it a promising technology for bone tissue engineering applications[8-10]. Both pore size and fiber diameter can be easily controlled by adjusting the printing parameters to meet the specific requirements of various tissues[11]. Several studies have demonstrated the benefits of utilizing MEW scaffolds in tissue engineering, such as wound healing, regeneration of periodontal tissue, and restoration of the acetabular labrum[12-14]. To date, limited research has been conducted on the utilization of MEW scaffolds for bone defect repair[15-17]. Therefore, additional investigations are needed to determine the effectiveness and potential applications of MEW scaffolds in craniofacial bone regeneration.

Recently, some synthetic polymers have been used to prepare MEW scaffolds, including polycaprolactone (PCL), poly (L-lactic acid) (PLLA), and polyethylene oxide (PEO)[18-20]. Of these, PCL is a highly desirable material due to its exceptional printability and low melting point[21]. It has been extensively utilized in numerous biological applications such as bone grafts, drug delivery systems, and skin grafts[22-24]. However, several studies have highlighted the weakness of PCL scaffold, particularly in bone integration after implantation, owing to its low cellular affinity[25,26]. Consequently, researchers have focused on improving the cytocompatibility of PCL.

Previous studies have shown that modifying the surface of a scaffold can improve its cellular affinity and cytocompatibility. This can be achieved through modifications in hydrophilicity, roughness, and morphology[27,28]. For example, the favorable hydrophilicity can facilitate cell adhesion and proliferation[29,30]. In addition, the specific micro/nanostructures on a surface and their appropriate roughness can have an impact on the attachment, morphology, spreading, and even differentiation of cells[31,32]. Currently, various methods have been attempted to enhance the surface properties of PCL[26,33,34]. One such method involves mixing varying proportions of nanohydroxyapatite with PCL to improve the biocompatibility and surface morphology of the scaffold[35]. Additionally, chitosan and hyaluronic acid have been utilized to improve the biocompatibility and hydrophilicity of PCL[36]. Furthermore, the application of calcium phosphate coating on the surface of PCL scaffolds has been shown to enhance biological activity[37]. Despite the potential benefits, the current problems in surface modification of PCL scaffolds lie in the complex procedures and relatively high cost. Therefore, there is a need to develop a more convenient and efficient method for this process.

Alkaline hydrolysis has been reported as a simple and effective method for surface modification[38]. Sodium hydroxide (NaOH) treatment is capable of not only adding functional groups to polymer surfaces, but also inducing surface porosity through etching. This capability is not commonly found in other surface modification techniques[38]. Thus, the dual action of NaOH makes it a suitable option for modifying the surface of PCL. It is worth noting that previous studies have primarily focused on examining the impact of alkaline treatment on the physicochemical properties and cytocompatibility of PCL[39-41]. However, there is limited research on the effects of alkaline treatment on the differentiation of bone marrow mesenchymal stem cells (BMSCs). Based on the interactions between BMSCs and scaffolds, it is hypothesized that surface modification mediated by NaOH treatment could induce osteogenic differentiation of BMSCs.

To verify this hypothesis, the effects of NaOH treatment on physicochemical properties of PCL scaffolds were investigated, including surface morphology, surface roughness, and hydrophilicity. Moreover, *in vitro* experiments were performed to assess the impact of NaOH treatment-mediated surface modification on osteogenic differentiation and the mechanisms behind it. Finally, *in vivo* experimentations were conducted to assess bone regeneration of surface-modified PCL scaffolds (Scheme 1).

2. Materials and methods

2.1. Scaffold preparation

The PCL scaffold was prepared using a commercial MEW printing platform (BioPioneer-1, Shaanxi Bioprintissue Medical Technologies Co., Ltd.). In brief, PCL pellets were loaded into a metal cartridge and melted at 90°C to obtain a homogeneous fluid. The scaffolds were then printed using a 26G nozzle at a voltage of -7 kV and a printing speed of 40 mm/s. The air pressure was set at 10 MPa, and the distance between the collector and nozzle was 4 mm.

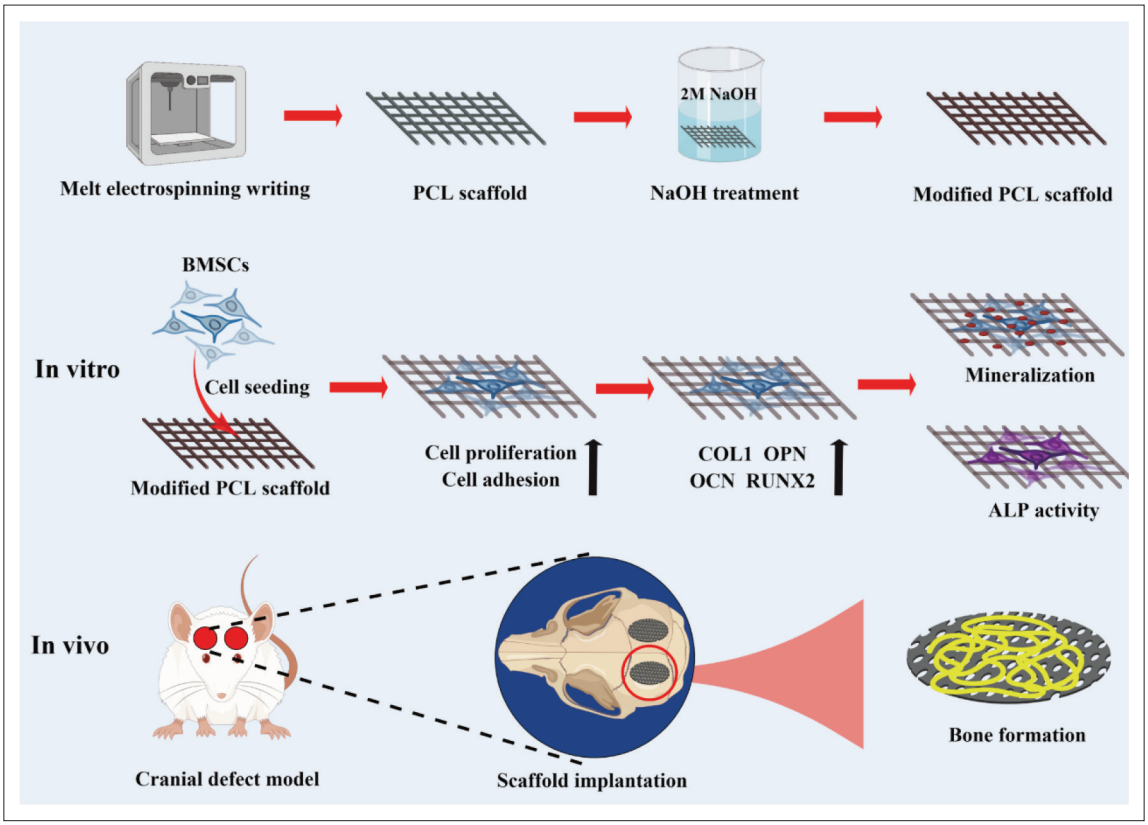

Scheme 1. Schematic diagram showing the osteogenic properties of surface-modified melt electrospinning writing (MEW) PCL scaffold. Abbreviations: ALP, alkaline phosphatase; BMSCs, bone marrow mesenchymal stem cells; NaOH, sodium hydroxide; PCL, polycaprolactone.

The entire process was carried out at a humidity level of 35% and an ambient temperature of 23°C. The printing parameters were determined using previous research as a guide[13,42].

2.2. NaOH treatment

NaOH was purchased from RHAWN company (Shanghai, China). The scaffolds were submerged in a 2 M NaOH solution within a 50 mL centrifuge tube and gently agitated on a laboratory shaker at 100 rpm for 1 h. The scaffolds were then rinsed with MilliQ water to neutralize the pH before being dried overnight in an oven set to 37°C.

2.3. Characterization of scaffold

2.3.1. Morphology

The morphology of scaffolds was detected by scanning electron microscopy (SEM, Thermo Fisher Scientific, USA). Briefly, the scaffolds were placed on the conductive glue and sprayed with a layer of gold. Electron dispersive X-ray diffraction (EDS) was used to evaluate the composition of elements of PCL scaffolds.

2.3.2. Surface roughness

Atomic force microscopy (AFM, Dimension Icon, Bruker, USA) technique was used to assess the surface roughness of scaffolds. To isolate the single fiber from scaffolds, it was then affixed to the tray using adhesive tape. The scanning area for all samples was consistent at 10 × 10 μm^2.

2.3.3. Surface wettability

Automatic contact angle system (JY-82B Kruss DSA) was used to evaluate surface wettability. To measure the water contact angle, a droplet of 5 μL distilled water was placed onto the scaffold, and its shape was subsequently photographed. Each sample was repeated three times.

2.3.4. Crystalline structures and chemical information

X-ray diffraction (XRD, BrukerAXS D8, USA) was used to analyze the crystalline structures of all scaffolds. XRD analysis was conducted with a 2θ range of 5–45° and speed rate of 2°/min. Fourier transform infrared (FTIR, Nicolet Is 10) analysis was performed to investigate chemical information. The sample collection was recorded from 600 to 4000 cm^{-1} a resolution of 4 cm^{-1}.

2.3.5 Mechanical properties

A uniaxial tensile test was conducted to assess the impact of NaOH treatment on the mechanical properties of PCL scaffold. The tensile Young's modulus and tensile strength were calculated between PCL and M-PCL groups.

2.4. Cell culture

Primary rat BMSCs were obtained from tibias and femurs of male Sprague-Dawley rats. BMSCs were culture in Modified Eagle Medium (MEM, Gibco, USA) supplemented with 10% fetal bovine serum (Biological industries, Australia). The cells were cultured at 37°C in a 5% CO_2 incubator. BMSCs of passages 3–6 were used for further experiments.

2.5. Cell proliferation, toxicity, and morphology

For cell experiments, the scaffolds were sterilized with 75% ethanol for 1 h and washed with phosphate-buffered saline (PBS) to remove residual ethanol. After that, BMSCs (2×10^5 cells) were seeded on the scaffolds in the 24-well plate. After 1, 4, and 7 days of culture, the cell proliferation was assessed with cell counting kit-8 (CCK-8, Beyotime, China). Briefly, 100 μL of CCK-8 solution was added to the cells and incubated for 30 min. The OD value at 540 nm was then detected using a microplate reader. Live/Dead staining kit was used for cytotoxicity analysis. In brief, the working solution was prepared with 2 μM calcein AM and 4.5 μM propidium iodide (PI) solution. After incubation for various time intervals, the cells on the scaffold were stained with a working solution for 15 min. Subsequently, the labeled cells were captured using immunofluorescence microscopy (Zeiss, Germany). Cell viability was calculated based on the ratio of the number of viable cells (green-stained cells) to the total number of cells (both green- and red-stained cells). For the quantification of results, three images per time point were analyzed using the ImageJ software for two groups. For morphology analysis, the BMSCs were fixed with glutaraldehyde and photographed by SEM.

2.6. Quantitative real-time PCR (qRT-PCR)

After being incubated at different time points, the BMSCs on the scaffold were digested by trypsin. Trizol reagent (Invitrogen, USA) was added into the 24-well plate to extract total RNA. The concentration of extracted RNA was detected using a microplate reader. The cDNA was synthesized by Reverse Transcription Kit (Takara, Dalian, China). The amplification process was conducted using the SYBR Taq Kit (Takara, Dalian, China). GAPDH was used as an internal reference. The primers are listed in **Table S1** (Supplementary File).

2.7. Immunofluorescence staining

After culturing on scaffolds for 7 and 14 days, the cells were fixed with 4% paraformaldehyde, permeabilized using Triton-X, and blocked with goat serum. Following this, the cells were incubated with primary antibodies (anti-OPN, 1:200, Proteintech; anti-OCN, 1:200, Proteintech; anti-RUNX2, 1:300, Proteintech) overnight at 4°C. Following the PBS wash, the cells were incubated with secondary antibodies for an hour at room temperature. The nuclei were then counterstained using DAPI, and the resulting images were captured using confocal microscopy (Nikon, Japan).

2.8. Western blotting

After being cultured on scaffolds for 14 days, the BMSCs were lysed using RIPA. The total proteins were then separated by gel electrophoresis, transferred to polyvinylidene fluoride membranes, and subsequently blocked with 5% milk. Following incubation with primary antibodies, the membranes were washed with TBST and treated with horseradish peroxidase-conjugated secondary antibodies. Finally, the membranes were photographed using Amersham Imager 600. Details of antibodies are listed in **Table S2** (Supplementary File).

2.9. Alizarin red S staining

After incubating for 14 and 21 days, the BMSCs on the scaffolds were washed with PBS and fixed with 4% paraformaldehyde for 20 min. Subsequently, the cells were stained with Alizarin red S staining solution (Beyotime, China) for 30 min at room temperature. Finally, the gross and optical images were photographed. For quantification analysis, the scaffolds were loaded into 5% sodium dodecyl sulfate (SDS) in 0.5 N HCl for 1 h at room temperature. The absorbance at 405 nm of this solution was measured using a microplate reader.

2.10. Alkaline phosphatase (ALP) staining and activity

The BCIP/NBT Alkaline Phosphatase Color Development Kit (Beyotime, China) was used for ALP staining. After being incubated for 7 and 14 days, the cells were fixed with 4% paraformaldehyde for 20 min and stained with working solution for 30 min. After that, the stain was washed with distilled water. In addition, Alkaline Phosphatase Assay Kit (Beyotime, China) was used for ALP activity analysis according to the manufacture's protocol. The absorbance at 405 nm was measured using a microplate reader.

2.11. Transcriptome sequencing

After being incubated for 14 days, the BMSCs on the scaffold were lysed using Trizol reagent (Invitrogen, USA) and the lysates were stored at -80°C for further experiments. Illumina NovaSeq 6000 was used to perform RNA sequencing. The criteria for screening differently expressed genes were $P < 0.05$ and $|\log2FoldChange| > 1$. Free online platform of Novogene was used to conduct Kyoto Encyclopedia of Genes and Genomes (KEGG) pathway enrichment analyses.

2.12. Animal experiments

The animal study was approved by Ethics Committees of The Fourth Military Medical University (IACUC-20220071). A

total of 36 male Sprague-Dawley rats (6-week-old, weighed 200 ± 10 g) were used in this study. To induce anesthesia, 1% pentobarbital (30 mg/kg) was administered to the rats. A midline sagittal incision was made to expose the skull, followed by the creation of a defect with 5 mm diameter on both sides of the parietal bones using a circular drill. Circular scaffolds measuring 1 mm in height and 5 mm in diameter were then inserted into the prepared defects. Finally, the incisions were closed, and the rats were allowed to recover in their cages. The Calcein-Alizarin red staining was performed to detect the newly formed bone.

2.12.1. Micro-computed tomography (micro-CT)

After 1 and 3 months of implantation, the rats were anesthetized and sacrificed. The samples were harvested and fixed with 4% paraformaldehyde. After that, the morphology analysis was detected using micro-CT. The bone volume to tissue volume (BV/TV), trabecular thickness (Tb.Th), and trabecular separation (Tb.Sp) were calculated to assess new bone formation.

2.12.2. Histological observation

The samples underwent decalcification with EDTA for a period of 6 weeks. Following this, they were dehydrated using 30% sucrose overnight. Ultimately, the samples were embedded in optimal cutting temperature (OCT) compound and sliced into 5-μm frozen sections. Mineralized bone formation was evaluated by hematoxylin and eosin (H&E) staining, Masson's trichrome staining, and immunochemical staining. For undecalcified bone, the samples were embedded in methylmethacrylate and sliced into 10-μm sections. After that, Alizarin Red S (red) and calcein (green) staining were photographed using confocal microscopy. Finally, the undecalcified slices were stained van Gieson's picrofuchsin.

2.13. Statistical analysis

All data were expressed as mean ± standard deviation. The comparison between the groups was performed by one-way ANOVA or *t*-test. A $P < 0.05$ was considered statistically significant.

3. Results

3.1. Physical properties of scaffolds

This study employed MEW to create 3D polymeric (PCL) scaffolds for bone regeneration. Previous studies have found that the alignment of fibers and pore size had significant impact on the differentiation of BMSCs. A scaffold with a 90° fiber architecture and a pore size of at least 300 μm has been found to be more effective for osteointegration[43,44]. However, it is important to note that increasing the pore size can lead to a decrease in the mechanical strength of the scaffold. To balance both osteointegration and mechanical strength, we chose a strand spacing of 300 μm for our scaffold. Therefore, we selected a scaffold geometry with a 90° fiber architecture and a pore size of 300 μm for our research. Besides, the geometry of the scaffolds used for both *in vitro* and *in vivo* experiments was the same in this study. The scaffolds exhibited a highly organized architecture composed of well-aligned fibers with an average strand spacing of 300 ± 25 μm and an average fiber diameter of 30 ± 0.6 μm, with a porosity of 91.3% (Figure 1A and B). In order to simplify the discussion, the pure PCL scaffolds and the PCL scaffolds treated with alkaline modification were respectively referred to as PCL and M-PCL scaffolds. The impact of alkaline treatment on the surface morphology of PCL was analyzed through SEM. Results showed that the surface of M-PCL scaffolds exhibited nanopits and nanogrooves, in contrast to the smooth surface of the PCL scaffolds. The average size of the nanopits was 200.87 ± 10.67 nm, while the lengths of the nanogrooves varied from a few hundred nanometers to microns (Figure 1C).

The study evaluated surface roughness and wettability using AFM and automatic water contact angle. The results showed that alkaline treatment resulted in a significant increase in the mean roughness average (Ra), which was confirmed through quantitative analysis (Figure 1D and E). Similarly, the surface wettability of PCL scaffolds was significantly enhanced through alkaline treatment, as evidenced by a decrease in water contact angles from 124 ± 0.5° for untreated PCL scaffolds to 43.45 ± 0.3° for M-PCL scaffolds (Figure 1F and G).

Crystalline structures and chemical information were analyzed using XRD, FTIR, and EDS techniques. The XRD results showed two characteristic peaks of PCL at 21.4° and 23.8°, respectively. The M-PCL exhibited a similar pattern (Figure 1H). The FTIR analysis of PCL showed peaks at 2946, 2865, and 1720 cm^{-1}, which correspond to asymmetric CH_2, symmetric CH_2, and C=O stretching. The presence of hydroxyl bonded to the end of PCL chain and hydrolysis of PCL after alkaline treatment was indicated by the observation of O-H stretching band at ≈ 1600 cm^{-1} in M-PCL (Figure 1I). Next, EDS was conducted to evaluate the elements on the scaffold. It was found that the surface of PCL and M-PCL was predominated by carbon (C) and oxygen (O) elements. However, the O/C ratio of PCL and M-PCL was 32.5% and 36.4%, respectively (Figure 1J and K). The rise in oxygen content following alkaline treatment suggests that M-PCL scaffolds have oxygen-containing functional groups, which is in line with the findings from the FTIR analysis.

Next, a uniaxial tensile test was conducted to assess the impact of NaOH treatment on the mechanical properties of PCL scaffold. The results revealed that both scaffolds

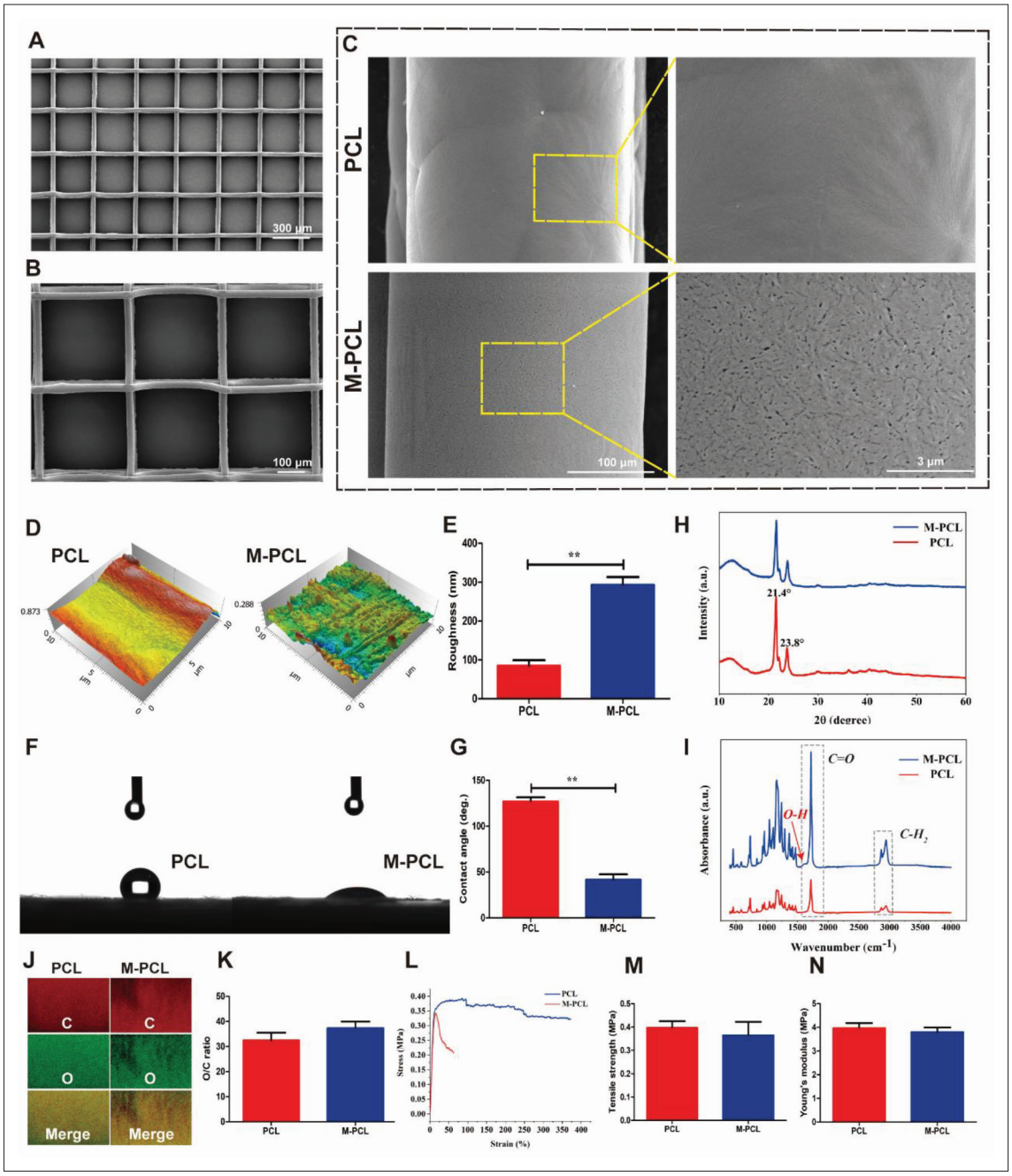

Figure 1. Characterizations of PCL scaffolds before and after alkaline treatment. (A, B) The morphology of PCL scaffolds at low and high magnification (SEM). (C) Surface morphology of PCL scaffolds before and after alkaline treatment. (D, E) AFM images of both scaffolds and quantification of surface roughness. (F, G) The water contact angles of both scaffolds and the quantitative results. (H) XRD spectrum of control and modified PCL scaffolds. (I) FTIR analysis of both scaffolds. (J, K) EDS elemental mapping for C and O, and the quantitative elemental analysis. (L) Stress–strain curves of two scaffolds. (M, N) Quantification of tensile strength and Young's modulus between two scaffolds. *$P < 0.05$, **$P < 0.01$.

displayed comparable fracture behavior. Initially, the scaffolds showed an elastic response, which was followed by significant plastic deformation before reaching failure (Figure 1L). Besides, the tensile strength and Young's modulus showed no significant difference between the PCL and M-PCL scaffolds (Figure 1M and N).

3.2. Effect of surface modification on cell compatibility

To assess the impact of alkaline treatment on cell compatibility, cell counting kit-8 (CCK-8) and live/dead assays were conducted to evaluate cell proliferation and viability. The findings indicate that the BMSCs grew

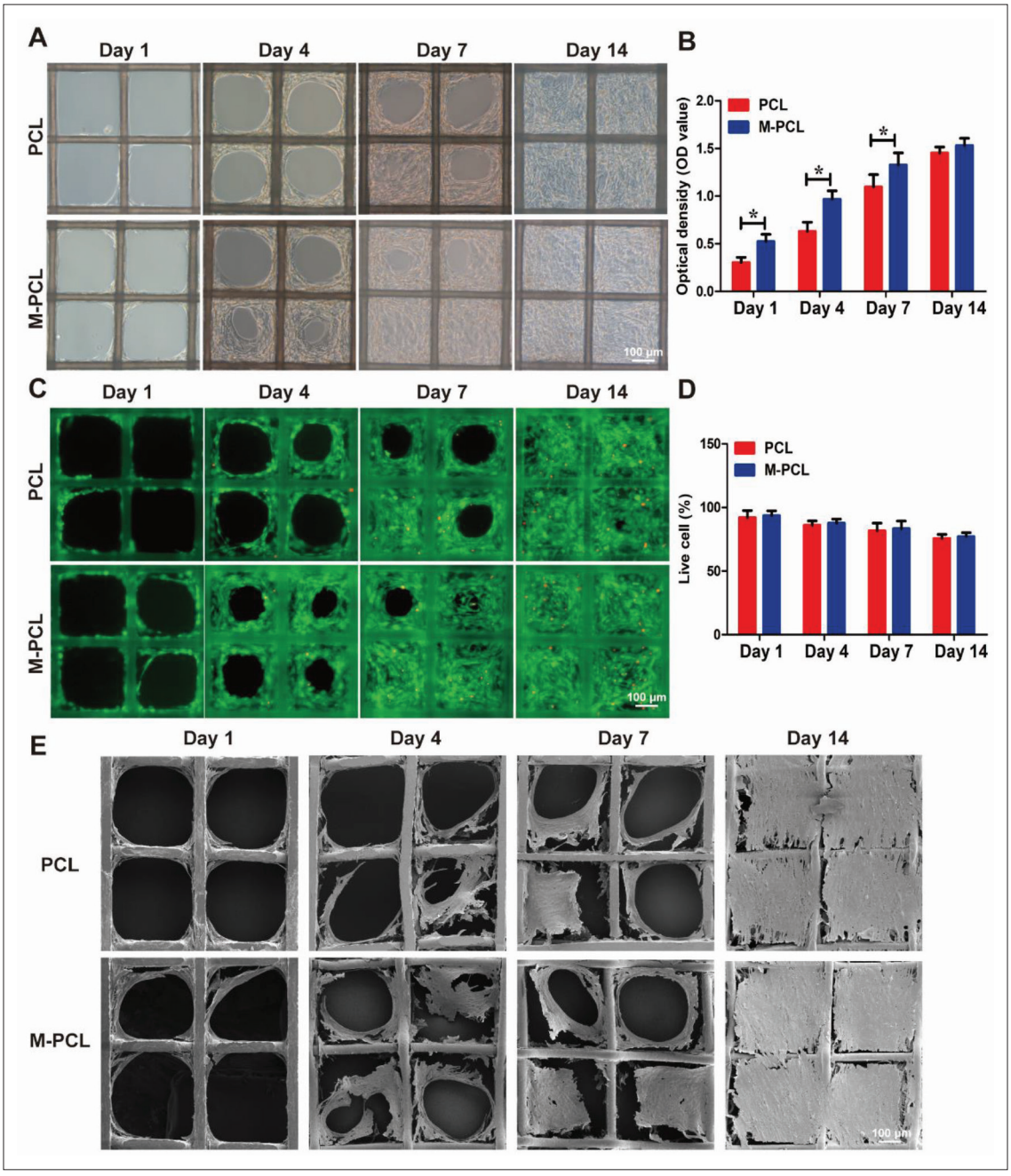

Figure 2. Biocompatibility of NaOH-treated PCL scaffolds. (A) Optical microscopy images of BMSCs on two different scaffolds. (B) Cell proliferation was assessed by CCK-8 assay. (C) The microscopy images of live/dead cells in two different groups. (D) Cell viability of BMSCs on two different scaffolds. (E) Representative SEM images of BMSCs at different times on PCL scaffolds. *$P < 0.05$, **$P < 0.01$.

from the peripheral sidewalls toward the center of the pore, eventually filling up all the pores in both groups (Figure 2A). According to the CCK-8 results, BMSCs exhibited a higher proliferation rate on the M-PCL scaffolds from day 1 to day 7. However, there was no significant difference in proliferation rate between the groups on day 14 (Figure 2B). The results of the live/dead test indicate that BMSCs on both scaffolds exhibited a high level of cell viability, approximately 90%, which then slightly decreased to 70%–80%. Furthermore, there was no significant difference in cell viability observed between the two groups (Figure 2C and D). Additionally, SEM images demonstrated that BMSCs initially adhered to the walls of the scaffolds and subsequently migrated toward the center, resulting in complete coverage of the scaffold (Figure 2E).

3.3. Effect of surface modification on cell morphology and adhesion

Cell morphology and adhesion were analyzed through double staining of vinculin (red) and F-actin (green). The cytoskeletons of BMSCs were observed to form a ring-shaped structure and interweave within the pores of all scaffolds (Figure 3A). In addition, the study found that BMSCs on M-PCL scaffolds produced a greater amount of vinculin compared to those on PCL scaffolds. This was confirmed through quantitative analysis of the average fluorescence intensity (Figure 3A and B). SEM results showed that BMSCs on M-PCL scaffolds displayed more and longer filopodial protrusions compared to relatively short and less filopodia on PCL scaffolds (Figure 3C).

3.4. Effect of surface modification on osteogenic differentiation

The study utilized qRT-PCR to detect the expression of osteogenesis-related genes such as collagen type 1 (*Col1*), osteocalcin (*Ocn*), osteopontin (*Opn*), and runt-related transcription factor 2 (*Runx2*). Results showed that, except for the *Col1* gene, the expressions of the other three genes were significantly higher in BMSCs cultured on M-PCL scaffolds than in BMSCs on PCL scaffolds after 7 days (Figure 4A), whereas the expression levels of all four genes were significantly higher at 14 days in M-PCL scaffolds compared to PCL scaffolds (Figure 4B). Immunofluorescence staining was used to measure the protein expression of OCN, OPN, and RUNX2. The results of the staining were consistent with those obtained from qRT-PCR. Specifically, the expressions of OCN, OPN, and RUNX2 proteins were observed to increase on PCL scaffolds following alkaline treatment (Figure 4C).

3.5 Effect of surface modification on mineralization and ALP activity

The study measured mineralization and ALP activity using ARD and ALP staining. BMSCs were cultured in basic medium without osteoinductive factors to determine the osteogenic capacity of the scaffolds. The depth of ARD staining was higher in M-PCL scaffolds compared to PCL scaffolds on days 14 and 21. Furthermore, there was more and larger calcium ion deposition and mineralization in the M-PCL scaffolds compared to PCL scaffolds (Figure 5A). These findings were also confirmed by quantitative analysis (Figure 5C). Similarly, the study found that M-PCL scaffolds had a higher level of ALP activity compared to PCL scaffolds after 7 and 14 days of culture (Figure 5B). Meanwhile, additionally, quantitative analysis of ALP staining confirmed that alkaline treatment of PCL scaffolds resulted in increased ALP activity (Figure 5D).

3.6. Surface modification mediated osteogenesis via integrinα2/β1-PI3K-AKT signaling pathway

Transcriptomics analysis identified 2116 differentially expressed genes (DEGs), with 1413 upregulated and 713 downregulated DEGs (Figure 6A and B). The underlying mechanisms were then analyzed using KEGG analyses, which revealed the top 20 KEGG pathways (Figure 6C). Previous studies have shown that the use of hierarchical microgroove/nanopore topography on titanium implants can improve osseointegration through the activation of the PI3K-AKT signaling pathway[45]. Therefore, it was chosen for subsequent study. Further analysis demonstrated a significant upregulation of gene expression in the PI3K-Akt signaling pathway in the M-PCL group compared to the PCL group (Figure 6D). Western blotting confirmed the activation of the PI3K-Akt signaling pathway (Figure 6E). These findings suggest that the NaOH-modified surface can enhance osteogenic differentiation through the integrinα2/β1-PI3K-Akt signaling pathway (Figure 6F).

3.7. Effect of surface modification on bone formation *in vivo*

In order to evaluate the effect of surface modification on bone formation of critical-sized bone defects, the rat cranial defect model was utilized. After 1 and 3 months of implantation, micro-CT 3D reconstruction was performed to assess new bone regeneration on scaffolds. The resulting micro-CT 3D images showed that there was a higher amount of newly formed bone on the M-PCL scaffolds than on the PCL scaffold at both 1 and 3 months (Figure 7A; **Figure S1** in Supplementary File). The results were further confirmed through quantitative analysis. It was observed that M-PCL scaffolds had a higher BV/TV value in comparison to PCL scaffolds (Figure 7B). Additionally, the new bone formed on M-PCL scaffolds exhibited improved trabecular structural features, which was confirmed by the quantitative analysis of Tb.Th and Tb.Sp (Figure 7C and D). To measure new bone formation, fluorescent double labeling of calcein (green) and Alizarin Red (red) was performed. The M-PCL scaffold showed a bigger distance between the two fluorescent signals (Figure 7E). Further quantitative analysis revealed that the mineral apposition rate (MAR) of M-PCL scaffolds was higher than that of PCL scaffolds (Figure 7F).

After a duration of 1 month, the control group showed thin fibrous tissue at the defect site. However, there was a stable integration between M-PCL scaffolds and host bone at the edge of the bone defect. Only a few scattered bone formations were noted in PCL scaffolds. After a period of 3 months, a higher amount of bone formation was observed in M-PCL scaffolds, resulting in a bony bridge at the defect

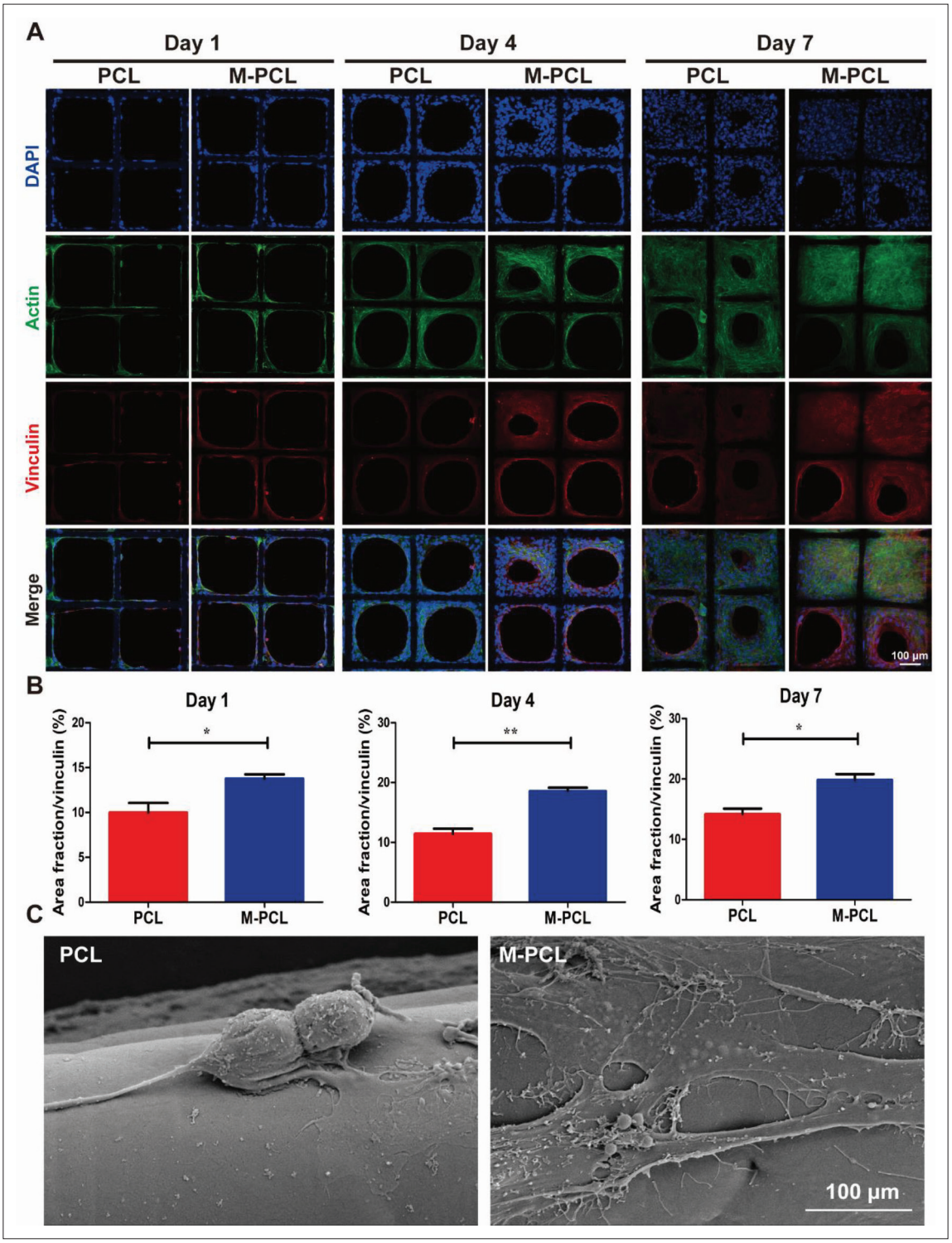

Figure 3. Effect of surface modification on cell morphology and adhesion. (A) Confocal microscopy images of actin (green) and vinculin (red) of BMSCs on different scaffolds. (B) Quantitative analysis of average fluorescence intensity of vinculin. (C) Representative SEM images of filopodial protrusions on different scaffolds.

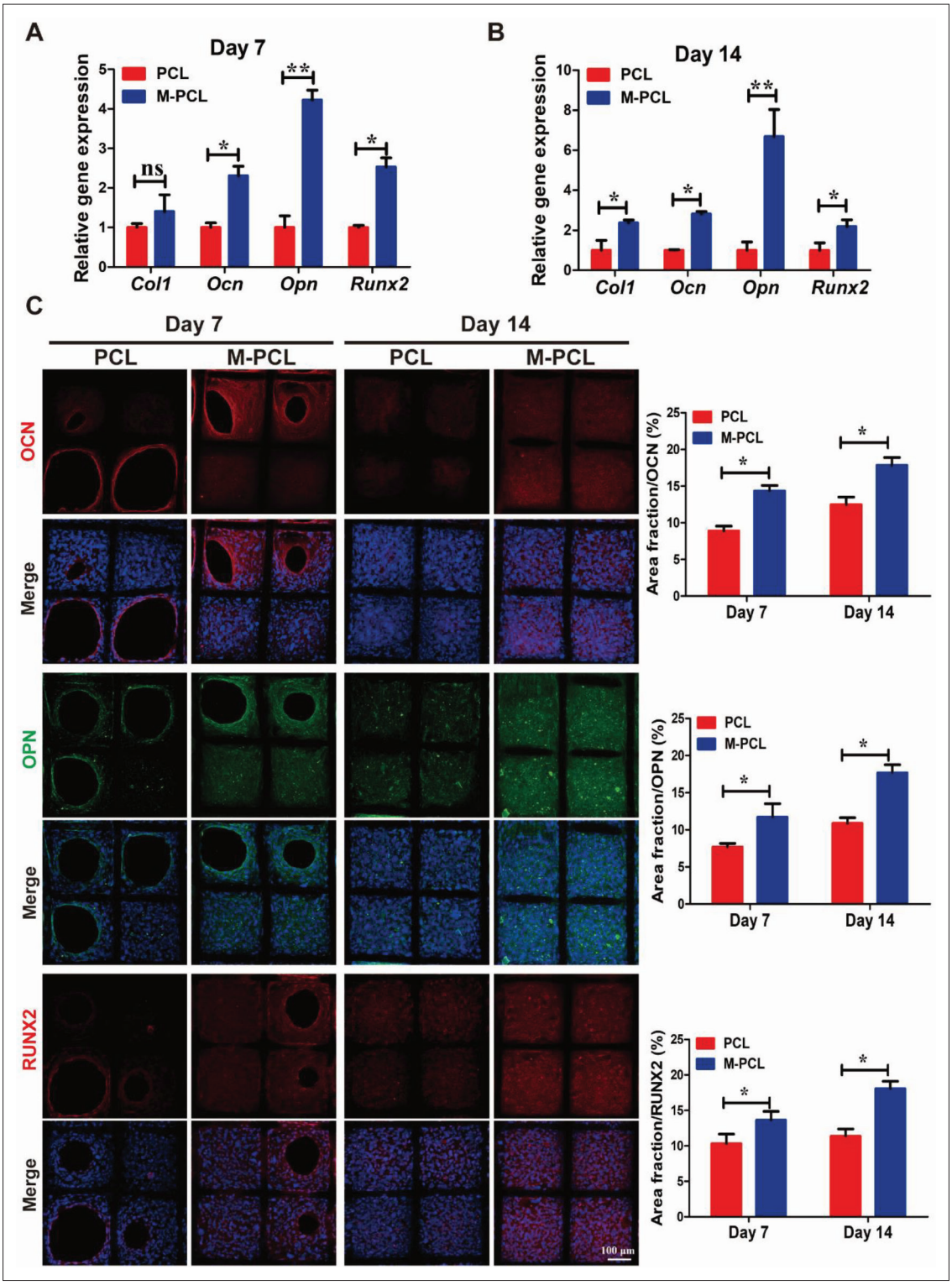

Figure 4. Effect of surface modification on osteogenic differentiation *in vitro*. (A, B) The gene expression of *Col1*, *Ocn*, *Opn*, and *Runx2* was examined using qRT-PCR after culture for 7 and 14 days. (C) The protein expressions of OCN, OPN, and RUNX2 were measured by immunofluorescence staining. $^{*}P < 0.05$, $^{**}P < 0.01$.

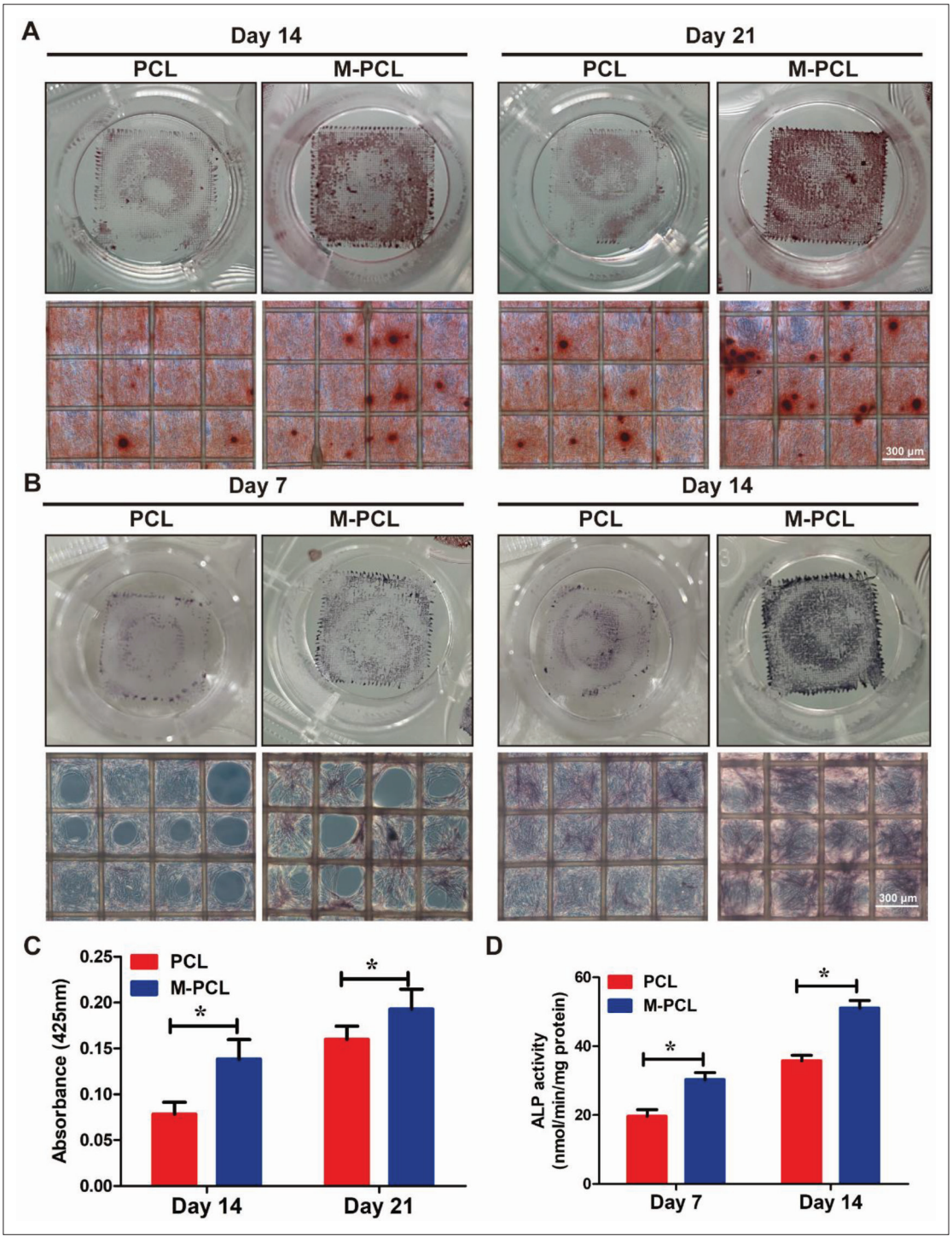

Figure 5. Effect of surface modification on mineralization and ALP activity. (A) Optical and microscopy images of ARD staining on PCL scaffold at 14 and 21 days. (B) Optical and microscopy images of ALP staining on PCL scaffold at 7 and 14 days. (C) Quantitative analysis of calcium ion deposition. (D) Quantitative analysis of ALP activity. *$P < 0.05$, **$P < 0.01$.

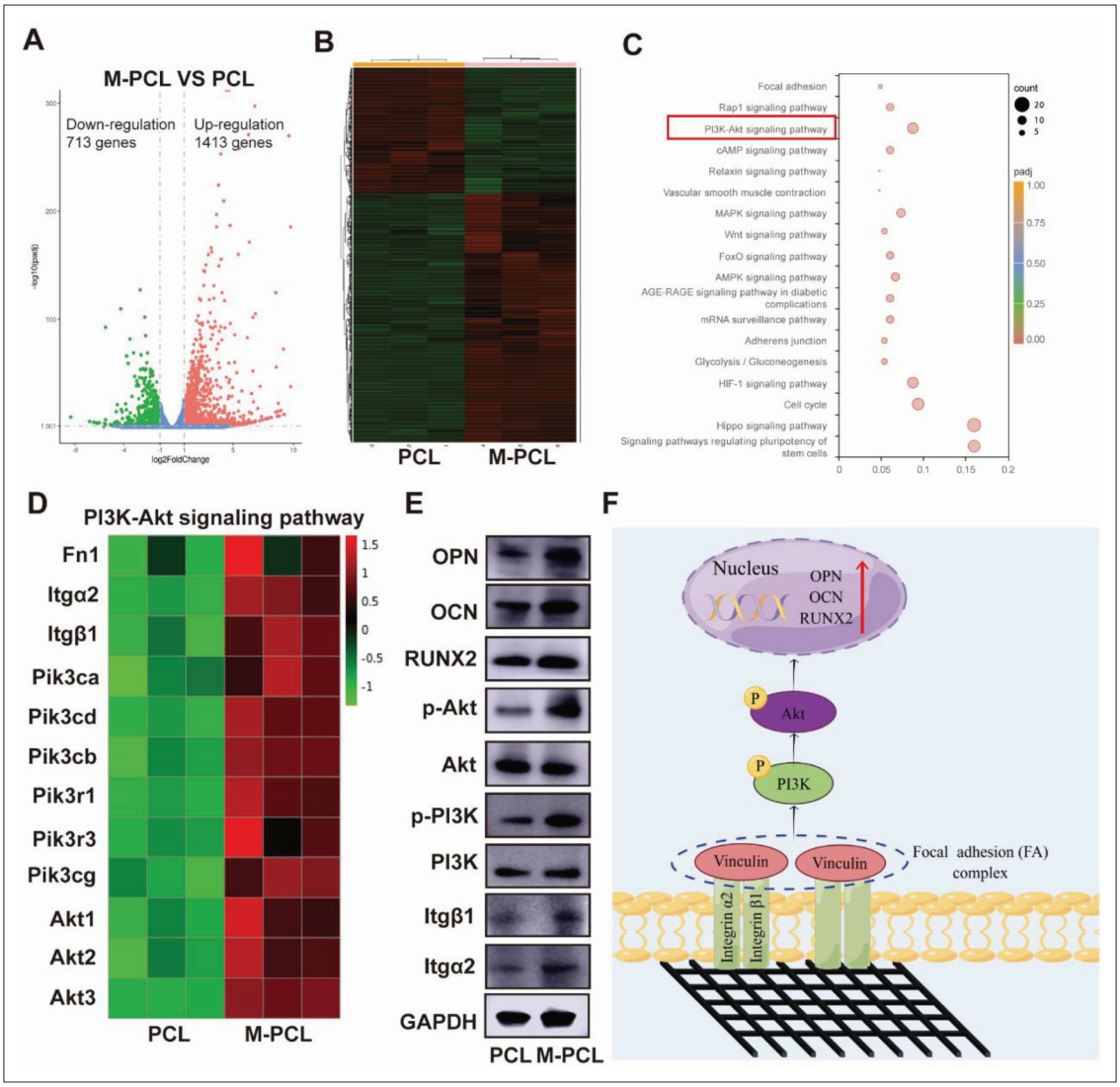

Figure 6. Surface modification mediated osteogenesis via integrinα2/β1-PI3K-AKT signaling pathway. (A) The scatter diagram of DEGs. (B) The heatmap of DEGs. (C) The top 20 KEGG signaling pathways. (D) The expression of genes in PI3K-Akt signaling pathway. (E) The expression of proteins in PI3K-Akt signaling pathway was detected by Western blotting. (F) Modified surface could facilitate osteogenic differentiation via integrinα2/β1-PI3K-Akt signaling pathway.

sites (Figure 7G). Furthermore, the presence of lamellar bone in M-PCL scaffolds was confirmed through Masson's trichrome staining (Figure 7H). Interestingly, van Gieson staining revealed an increased number of bone calluses in M-PCL scaffolds, which is consistent with the findings of H&E and Masson's trichrome staining (**Figure S2** in Supplementary File).

Immunohistochemical staining was utilized to quantify the levels of OPN, OCN, and RUNX2 protein. After a duration of 1 month, the results indicated that the levels of these three proteins were higher in M-PCL scaffolds compared to PCL scaffolds (Figure 8A, C, and E). As time went by, protein expression of OPN, OCN, and RUNX2 decreased in both scaffolds at 3 months. Besides, the difference in protein expression between PCL and M-PCL scaffolds was less pronounced at this point (Figure 8A–F).

4. Discussion

This study aimed to explore the impact of surface modification through alkaline treatment on the osteoinductive properties of MEW PCL scaffolds. PCL has been extensively utilized for creating biocompatible scaffolds for tissue engineering, particularly for bone tissue engineering scaffolds[46]. The limitations of PCL in tissue engineering arise from its surface hydrophobicity and inertness, which are not conducive to cell proliferation and

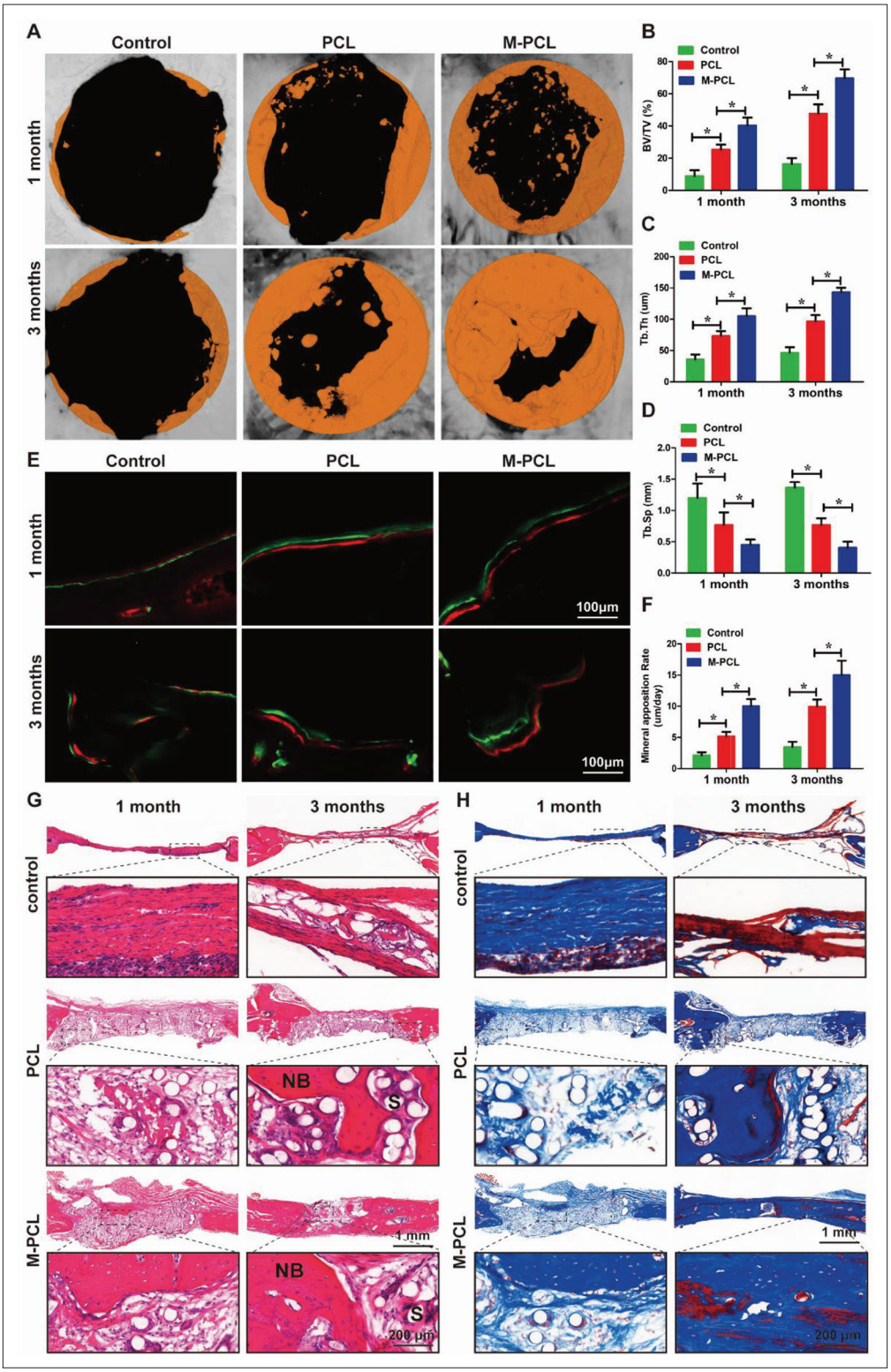

Figure 7. Micro-CT analysis, sequential fluorescent labeling, and histological analysis of new bone formation. (A) Micro-CT 3D images of PCL scaffolds. (B) Quantitative analysis of BV/TV value after implantation for 1 and 3 months. (C, D) Quantitative analysis of bone formation according to Tb.Th and Tb.Sp. (E) The newly formed bone was stained using calcein-Alizarin Red. (F) Quantitative analysis of mineral apposition rate. (G) H&E staining of the decalcified sections. (H) Masson's trichrome staining of the decalcified sections. $^{*}P < 0.05$, $^{**}P < 0.01$.

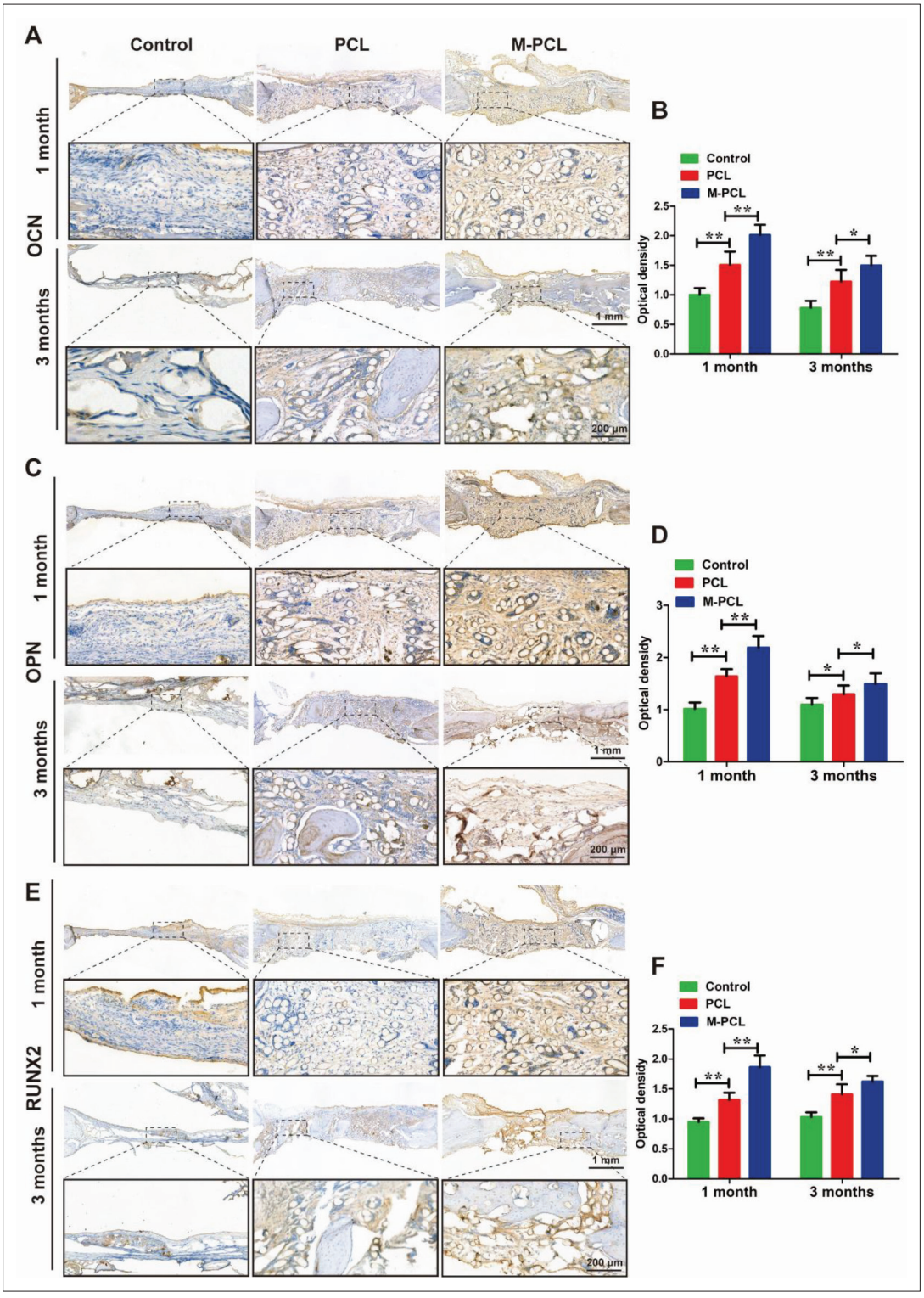

Figure 8. The protein expression of OCN, OPN, and RUNX2 in defect area. (A, B) The protein expressions of OCN and semi-quantification at 1 and 3 months after implantation. (C, D) The protein expression of OPN and semi-quantification at 1 and 3 months after implantation. (E, F) The protein expression of RUNX2 and semi-quantification at 1 and 3 months after implantation.

growth[22,26]. In order to improve the interaction between scaffolds and tissues, several methods have been employed to enhance the surface properties of PCL. These methods include covalent grafting, plasma treatment, and surface coating[33,34,38]. Of these, alkaline treatment stands out as a simple and effective way to modify both the physical and biological properties of scaffolds.

Compared to bulk hydrolysis, NaOH treatment is a surface hydrolysis method with a slower rate of NaOH diffusion into the polymer matrix, resulting in a higher surface hydrolysis rate[41]. It has been reported that the bulk properties of the scaffolds remained unchanged despite the hydrolysis treatment[13,38]. The present study utilized XRD, FTIR, and EDS to investigate the crystalline structures and chemical information of scaffolds, with a focus on the effects of surface hydrolysis. The results of FTIR analysis showed that hydroxyl groups bound to the PCL chain following NaOH treatment. However, XRD analysis indicated that the pattern of M-PCL was similar to that of PCL, suggesting that the crystallinity of both scaffolds remained similar after NaOH treatment. These findings confirm that NaOH treatment did not alter the bulk chain of PCL and was an effective surface modification strategy.

According to reports, the application of alkaline treatment has an impact on certain physical properties of PCL such as surface wettability, roughness, and morphology[38,40]. The surface of PCL undergoes a breakage of ester bonds when treated with NaOH, leading to the formation of functional hydroxyl and carboxyl groups. This process ultimately enhances the hydrophilicity of PCL[47]. The AFM analysis results indicated that the surface roughness of PCL scaffolds increased after NaOH treatment, which could be attributed to the alteration in surface morphology. SEM images revealed that the surface of M-PCL scaffolds exhibited a rough microstructure due to the presence of nanopits and nanogrooves, whereas the surface of PCL scaffolds appeared smooth.

In addition to physical properties, the biological properties of PCL can also be affected by alkaline treatment-mediated surface modification. As a result, we conducted further investigation to determine the impact of surface modification on cell proliferation, viability, and adhesion. It is widely recognized that the low surface hydrophilicity of PCL hinders cell proliferation[41]. The surface hydrophilicity of PCL scaffolds was increased after NaOH treatment, leading to a higher proliferation rate of BMSCs on M-PCL scaffolds from days 1 through 7. However, there was no significant difference in the proliferation rate between the two groups on day 14. This may be due to the fact that the pores of both scaffolds were filled with cells, leaving no additional space for further cell proliferation. Besides, the results of the live/dead test suggest that surface modification did not have a negative impact on cell viability, as there was no significant difference in cell viability between the two groups. Vinculin, a protein found in focal adhesions (FA), is closely linked to a cell's adhesive capacity[48]. The current study demonstrated that BMSCs grown on M-PCL scaffolds produce more vinculin and filopodial protrusions compared to those grown on PCL scaffolds. This may be attributed to the presence of nanopits and nanogrooves on the M-PCL scaffolds, which offer more anchoring points for cells.

Finally, we investigated the impact of surface modification on the osteoinductive properties of PCL scaffolds. Our findings revealed that M-PCL scaffolds could enhance the expression of osteogenesis-related genes, mineralization, and ALP activity *in vitro*, as well as promote bone formation *in vivo*. Previous research has only focused on evaluating the effects of alkaline treatment on the physicochemical properties and cytocompatibility of PCL. This study is the first to explore the underlying mechanism behind the osteoinductive effects of NaOH-treated PCL scaffolds. Previous studies have found that 3D-printed titanium scaffolds with a surface roughness of approximately 110–1300 nm can promote osteogenic differentiation of BMSCs[49-51]. According to reports, filopodial protrusions have the ability to initiate integrin clustering and recruit focal adhesion (FA) proteins. This process transforms mechanical signals into chemical signals, ultimately leading to stem cell differentiation[45]. In this study, the surface roughness of M-PCL was found to be approximately 300 nm, which falls within the desired size range. Furthermore, BMSCs on M-PCL scaffolds exhibited a greater number of filopodial protrusions that were longer in length. Based on these results, it can be inferred that the surface-modified PCL scaffolds possess an optimal surface roughness that facilitates filopodia anchoring and subsequently influences downstream signaling pathways to promote osteogenic differentiation. However, the mechanisms behind the osteogenic properties of surface-modified PCL scaffolds were unclear. To investigate this, transcriptome analysis was performed. The results showed that the alkaline treatment-modified surface facilitated osteogenic differentiation through the integrinα2/β1-PI3K-Akt signaling pathway. Altogether, the results suggest that alkaline treatment is a straightforward and efficient technique to improve the osteogenic properties of MEW PCL scaffolds.

5. Conclusion

This study introduces a simple and effective NaOH treatment method to improve the bioactivity of the MEW PCL scaffold. The treatment increases the surface wettability and

roughness of PCL scaffolds, making them favorable for cell proliferation and adhesion. Additionally, osteoinductive properties were enhanced *in vitro* and *in vivo*, likely due to modified surface-mediated enhancement of osteogenic differentiation via the integrinα2/β1-PI3K-Akt signaling pathway. These findings suggest that NaOH treatment is a cost-efficient and effective strategy for surface modification of PCL scaffolds in bone tissue regeneration.

Acknowledgments

We acknowledge Mrs. Xiaoli Qu for helping the team use immunofluorescence microscopy (State Key Laboratory for Manufacturing Systems Engineering, Xi'an Jiaotong University). The Figdraw was acknowledged for producing Scheme 1 and Figure 6F.

Funding

This work was supported by National Natural Science Foundation of China (No. 31971272) and International Science and Technology Cooperation Keg Program project of Shaanxi Province (No. 2023-GHZD-25).

Conflict of interest

The authors declare no conflicts of interests.

Author contributions

Conceptualization: Hongbin Fan
Formal analysis: Jingyi Dang, Zhao Zhang
Methodology: Yubo Shi, Lei Wang
Resources: Jiankang He, Zhennan Qiu, Xiaoli, Qu
Writing – original draft: Yubo Shi, Liguo Sun
Writing – review & editing: Yubo Shi, Hongbin Fan

Ethics approval and consent to participate

The animal study was approved by Ethics Committees of The Fourth Military Medical University (IACUC-20220071).

Consent for publication

Not applicable.

Availability of data

The request for raw data can be directed to the corresponding author.

References

1. Maruyama T, Stevens R, Boka A, *et al.*, 2021, BMPR1A maintains skeletal stem cell properties in craniofacial development and craniosynostosis. *Sci Transl Med*, 13(583): eabb4416.

   https://doi.org/10.1126/scitranslmed.abb4416

2. Stahl A, Yang YP, 2021, Regenerative approaches for the treatment of large bone defects. *Tissue Eng Part B Rev*, 27(6): 539–547.

   https://doi.org/10.1089/ten.TEB.2020.0281

3. Dimitriou R, Jones E, Mcgonagle D, *et al.*, 2011, Bone regeneration: Current concepts and future directions. *BMC Med*, 9: 66.

   https://doi.org/10.1186/1741-7015-9-66.

4. Azi ML, Aprato A, Santi I, *et al.*, 2016, Autologous bone graft in the treatment of post-traumatic bone defects: A systematic review and meta-analysis. *BMC Musculoskelet Disord*, 17(1): 465.

   https://doi.org/10.1186/s12891-016-1312-4

5. Charbe NB, Tambuwala M, Palakurthi SS, *et al.*, 2023, Biomedical applications of three-dimensional bioprinted craniofacial tissue engineering. *Bioeng Transl Med*, 8(1): e10333.

   https://doi.org/10.1002/btm2.10333

6. Shi Y, Yu L, Gong C, *et al.*, 2021, A bioactive magnesium phosphate cement incorporating chondroitin sulfate for bone regeneration. *Biomed Mater*, 16(3).

   https://doi.org/10.1088/1748-605X/abf5c4

7. Roseti L, Parisi V, Petretta M, *et al.*, 2017 Scaffolds for bone tissue engineering: State of the art and new perspectives. *Mater Sci Eng C Mater Biol Appl*, 78: 1246–1262.

   https://doi.org/10.1016/j.msec.2017.05.017

8. Wunner FM, Wille ML, Noonan TG, *et al.*, 2018, Melt electrospinning writing of highly ordered large volume scaffold architectures. *Adv Mater*, 30(20): e1706570.

   https://doi.org/10.1002/adma.201706570

9. Kade JC, Dalton PD, 2021, Polymers for melt electrowriting. *Adv Healthc Mater*, 10(1): e2001232.

   https://doi.org/10.1002/adhm.202001232

10. Chen Z, Liu Y, Huang J, *et al.*, 2022, Influences of process parameters of near-field direct-writing melt electrospinning on performances of polycaprolactone/nano-hydroxyapatite scaffolds. *Polymers (Basel)*, 14(16): 3404.

    https://doi.org/10.3390/polym14163404

11. He J, Zhang B, Li Z, *et al.*, 2020, High-resolution electrohydrodynamic bioprinting: A new biofabrication strategy for biomimetic micro/nanoscale architectures and living tissue constructs. *Biofabrication*, 12(4): 042002.

    https://doi.org/10.1088/1758-5090/aba1fa

12. Mirzaei M, Dodi G, Gardikiotis I, *et al.*, 2023, 3D high-precision melt electro written polycaprolactone modified with yeast derived peptides for wound healing. *Biomater Adv*, 149: 213361.

    https://doi.org/10.1016/j.bioadv.2023.213361

13. Daghrery A, Ferreira JA, De Souza Araújo IJ, *et al.*, 2021, A highly ordered, nanostructured fluorinated CaP-coated melt electrowritten scaffold for periodontal tissue regeneration. *Adv Healthc Mater*, 10(21): e2101152.

    https://doi.org/10.1002/adhm.202101152

14. Santschi MXT, Huber S, Bujalka J, *et al.*, 2022, Mechanical and biological evaluation of melt-electrowritten polycaprolactone scaffolds for acetabular labrum restoration. *Cells*, 11(21): 3450.

    https://doi.org/10.3390/cells11213450

15. Eichholz KF, Freeman FE, Pitacco P, *et al.*, 2022, Scaffold microarchitecture regulates angiogenesis and the regeneration of large bone defects. *Biofabrication*, 14(4).

    https://doi.org/10.1088/1758-5090/ac88a1

16. Steele JaM, Moore AC, St-Pierre JP, *et al.*, 2022, In vitro and in vivo investigation of a zonal microstructured scaffold for osteochondral defect repair. *Biomaterials*, 286: 121548.

    https://doi.org/10.1016/j.biomaterials.2022.121548

17. Abbasi N, Lee RSB, Ivanovski S, *et al.*, 2020, In vivo bone regeneration assessment of offset and gradient melt electrowritten (MEW) PCL scaffolds. *Biomater Res*, 24: 17.

    https://doi.org/10.1186/s40824-020-00196-1

18. Daghrery A, De Souza Araújo IJ, Castilho M, *et al.*, 2023, Unveiling the potential of melt electrowriting in regenerative dental medicine. *Acta Biomater*, 156: 88–109.

    https://doi.org/10.1016/j.actbio.2022.01.010

19. Jing L, Wang X, Leng B, *et al.*, 2021, Engineered nanotopography on the microfibers of 3D-printed PCL scaffolds to modulate cellular responses and establish an in vitro tumor model. *ACS Appl Bio Mater*, 4(2): 1381–1394.

    https://doi.org/10.1021/acsabm.0c01243

20. Meng J, Boschetto F, Yagi S, *et al.*, 2022, Enhancing the bioactivity of melt electrowritten PLLA scaffold by convenient, green, and effective hydrophilic surface modification. *Mater Sci Eng C Mater Biol Appl*, 135: 112686.

    https://doi.org/10.1016/j.msec.2022.112686

21. Rasperini G, Pilipchuk SP, Flanagan CL, *et al.*, 2015, 3D-printed bioresorbable scaffold for periodontal repair. *J Dent Res*, 94: 153s–157s.

    https://doi.org/10.1177/0022034515588303

22. Wong HM, Wu S, Chu PK, *et al.*, 2013, Low-modulus Mg/PCL hybrid bone substitute for osteoporotic fracture fixation. *Biomaterials*, 34(29): 7016–7032.

    https://doi.org/10.1016/j.biomaterials.2013.05.062

23. Feng B, Tu H, Yuan H, *et al.*, 2012, Acetic-acid-mediated miscibility toward electrospinning homogeneous composite nanofibers of GT/PCL. *Biomacromolecules*, 13(12): 3917–3925.

    https://doi.org/10.1021/bm3009389

24. Zhou Q, Zhang H, Zhou Y, *et al.*, 2017, Alkali-mediated miscibility of gelatin/polycaprolactone for electrospinning homogeneous composite nanofibers for tissue scaffolding. *Macromol Biosci*, 17(12).

    https://doi.org/10.1002/mabi.201700268

25. Zheng R, Duan H, Xue J, *et al.*, 2014, The influence of Gelatin/PCL ratio and 3-D construct shape of electrospun membranes on cartilage regeneration. *Biomaterials*, 35(1): 152–164.

    https://doi.org/10.1016/j.biomaterials.2013.09.082

26. Jing X, Mi HY, Wang XC, *et al.*, 2015, Shish-kebab-structured poly(ε-caprolactone) nanofibers hierarchically decorated with chitosan-poly(ε-caprolactone) copolymers for bone tissue engineering. *ACS Appl Mater Interfaces*, 7(12): 6955–6965.

    https://doi.org/10.1021/acsami.5b00900

27. Jin S, Yang R, Chu C, *et al.*, 2021, Topological structure of electrospun membrane regulates immune response, angiogenesis and bone regeneration. *Acta Biomater*, 129: 148–158.

    https://doi.org/10.1016/j.actbio.2021.05.042

28. Hao M, Liu Y, Chen Z, *et al.*, 2022, Cross-linked gamma polyglutamic acid/human hair keratin electrospun nanofibrous scaffolds with excellent biocompatibility and biodegradability. *Polymers (Basel)*, 14(24): 5505.

    https://doi.org/10.3390/polym14245505

29. Crowder SW, Leonardo V, Whittaker T, *et al.*, 2016, Material cues as potent regulators of epigenetics and stem cell function. *Cell Stem Cell*, 18(1): 39–52.

    https://doi.org/10.1016/j.stem.2015.12.012

30. Lv L, Tang Y, Zhang P, *et al.*, 2018, Biomaterial cues regulate epigenetic state and cell functions-A systematic review. *Tissue Eng Part B Rev*, 24(2): 112–132.

    https://doi.org/10.1089/ten.teb.2017.0287

31. Veiseh O, Doloff JC, Ma M, *et al.*, 2015, Size- and shape-dependent foreign body immune response to materials implanted in rodents and non-human primates. *Nat Mater*, 14(6): 643–651.

    https://doi.org/10.1038/nmat4290

32. Leal-Egaña A, Díaz-Cuenca A, Boccaccini AR, 2013, Tuning of cell-biomaterial anchorage for tissue regeneration. *Adv Mater*, 25(29): 4049–4057.

    https://doi.org/10.1002/adma.201301227

33. Yeo A, Wong WJ, Teoh SH, 2010, Surface modification of PCL-TCP scaffolds in rabbit calvaria defects: Evaluation of scaffold degradation profile, biomechanical properties and bone healing patterns. *J Biomed Mater Res A*, 93(4): 1358–1367.

    https://doi.org/10.1002/jbm.a.32633

34. Tiaw KS, Goh SW, Hong M, *et al.*, 2005, Laser surface modification of poly(epsilon-caprolactone) (PCL) membrane for tissue engineering applications. *Biomaterials*, 26(7): 763–769.

https://doi.org/10.1016/j.biomaterials.2004.03.010

35. Chen Z, Liu Y, Huang J, *et al.*, 2022, Enhanced in vitro biocompatible polycaprolactone/nano-hydroxyapatite scaffolds with near-field direct-writing melt electrospinning technology. *J Funct Biomater*, 13(4): 161.

https://doi.org/10.3390/jfb13040161

36. Chen Z, Hao M, Qian X, *et al.*, 2021, Characterization on modification and biocompatibility of PCL scaffold prepared with near-field direct-writing melt electrospinning. *Chem Res Chin Univ*, 37(3): 578–583.

https://doi.org/10.1007/s40242-021-1129-z

37. Vaquette C, Ivanovski S, Hamlet SM, *et al.*, 2013, Effect of culture conditions and calcium phosphate coating on ectopic bone formation. *Biomaterials*, 34(22): 5538–5551.

https://doi.org/10.1016/j.biomaterials.2013.03.088

38. Gupta D, Singh AK, Kar N, *et al.*, 2019, Modelling and optimization of NaOH-etched 3-D printed PCL for enhanced cellular attachment and growth with minimal loss of mechanical strength. *Mater Sci Eng C Mater Biol Appl*, 98: 602–611.

https://doi.org/10.1016/j.msec.2018.12.084

39. Zamani Y, Mohammadi J, Amoabediny G, *et al.*, 2018, Enhanced osteogenic activity by MC3T3-E1 pre-osteoblasts on chemically surface-modified poly(ε-caprolactone) 3D-printed scaffolds compared to RGD immobilized scaffolds. *Biomed Mater*, 14(1): 015008.

https://doi.org/10.1088/1748-605X/aaeb82

40. Zhou ZX, Chen YR, Zhang JY, *et al.*, 2020, Facile strategy on hydrophilic modification of poly(ε-caprolactone) scaffolds for assisting tissue-engineered meniscus constructs in vitro. *Front Pharmacol*, 11: 471.

https://doi.org/10.3389/fphar.2020.00471

41. Lam CX, Hutmacher DW, Schantz JT, *et al.*, 2009, Evaluation of polycaprolactone scaffold degradation for 6 months in vitro and in vivo. *J Biomed Mater Res A*, 90(3): 906–919.

https://doi.org/10.1002/jbm.a.32052

42. Yao C, Qiu Z, Li X, *et al.*, 2023, Electrohydrodynamic printing of microfibrous architectures with cell-scale spacing for improved cellular migration and neurite outgrowth. *Small*, 19(19): e2207331.

https://doi.org/10.1002/smll.202207331

43. Eichholz KF, Hoey DA, 2018, Mediating human stem cell behaviour via defined fibrous architectures by melt electrospinning writing. *Acta Biomater*, 75: 140–151.

https://doi.org/10.1016/j.actbio.2018.05.048

44. Karageorgiou V, Kaplan D, 2005, Porosity of 3D biomaterial scaffolds and osteogenesis. *Biomaterials*, 26(27): 5474–5491.

https://doi.org/10.1016/j.biomaterials.2005.02.002

45. Tian Y, Zheng H, Zheng G, *et al.*, 2022, Hierarchical microgroove/nanopore topography regulated cell adhesion to enhance osseointegration around intraosseous implants in vivo. *Biomater Sci*, 10(2): 560–580.

https://doi.org/10.1039/d1bm01657a

46. Zhang P, Chen J, Sun Y, *et al.*, 2023, A 3D multifunctional bi-layer scaffold to regulate stem cell behaviors and promote osteochondral regeneration. *J Mater Chem B*, 11(6): 1240–1261.

https://doi.org/10.1039/d2tb02203f

47. Shegarfi H, Reikeras O, 2009, Review article: Bone transplantation and immune response. *J Orthop Surg (Hong Kong)*, 17(2): 206–211.

https://doi.org/10.1177/230949900901700218

48. Kanchanawong P, Shtengel G, Pasapera AM, *et al.*, 2010, Nanoscale architecture of integrin-based cell adhesions. *Nature*, 468(7323): 580–594.

https://doi.org/10.1038/nature09621

49. Prasopthum A, Cooper M, Shakesheff KM, *et al.*, 2019, Three-dimensional printed scaffolds with controlled micro-/nanoporous surface topography direct chondrogenic and osteogenic differentiation of mesenchymal stem cells. *ACS Appl Mater Interfaces*, 11(21): 18896–18906.

https://doi.org/10.1021/acsami.9b01472

50. Kumar G, Waters MS, Farooque TM, *et al.*, 2012, Freeform fabricated scaffolds with roughened struts that enhance both stem cell proliferation and differentiation by controlling cell shape. *Biomaterials*, 33(16): 4022–4030.

https://doi.org/10.1016/j.biomaterials.2012.02.048

51. Neves SC, Mota C, Longoni A, *et al.*, 2016, Additive manufactured polymeric 3D scaffolds with tailored surface topography influence mesenchymal stromal cells activity. *Biofabrication*, 8(2): 025012.

https://doi.org/10.1088/1758-5090/8/2/025012